

Radar Cross Section Measurements Using Terahertz Waves

Krzysztof Iwaszczuk¹, Henning Heiselberg², Peter Uhd Jepsen¹

- 1) DTU Fotonik – Department of Photonics Engineering, Technical University of Denmark, DK – 2800 Kongens Lyngby, Denmark
- 2) Danish Defense Acquisition & Logistics Organization, DK – 2750 Ballerup, Denmark

kiwa@fotonik.dtu.dk

Abstract: Radar cross sections at terahertz frequencies are measured on scale models of aircrafts. A time domain broadband THz system generates freely propagating THz pulses measured with sub-picosecond time resolution. The THz radiation is generated using fs laser pulses by optical rectification in a lithium niobate crystal with application of the tilted wave front method, resulting in high electric field THz pulses with a broad band spectrum from 100 GHz up to 4 THz. The corresponding wave lengths are two orders of magnitude smaller than normal radars and we therefore use scale models of size 5-10 cm in order to measure realistic radar cross sections. RCS polar and azimuthal angle plots of F-16 and F-35.

References and links

1. R. A. Cheville and D. Grischkowsky, "Time domain terahertz impulse ranging studies," *Appl. Phys. Lett.* **67**, 1960 (1995)
2. R. A. Cheville, R. W. McGowan and D. R. Grischkowsky, "Late-time target response measured with terahertz impulse ranging," *IEEE Trans. Antennas Propag.* **45**, 1518 (1997)
3. J. Pearce, H. Choi, D. M. Mittleman, J. White and D. Zimdars, "Terahertz wide aperture reflection tomography," *Opt. Lett.* **30**, 1653 (2005)
4. K. McClatchey, M. T. Reiten, and R.A. Cheville, "Time resolved synthetic aperture terahertz impulse imaging", *Appl. Phys. Lett.* **27**, 4485 (2001)
5. T. M. Goyette, J. C. Dickinson, J. Waldman, W. E. Nixon, "A 1.56THz compact radar range for W-band imagery of scale-model tactical targets," *Proc. SPIE, Algorithms for Synthetic Aperture Radar Imagery VII*, **4053**, 615 (2000)
6. X. J. Zhong, T. J. Cui and Z. Li, "Terahertz-wave scattering by perfectly electrical conducting objects," *J. Electromagn. Waves Appl.* **21**, 2331 (2007)
7. J. Pearce and D. M. Mittleman, "Scale model experimentation: using terahertz pulses to study light scattering," *Phys. Med. Biol.* **47**, 3823 (2002)
8. J. Pearce, D. M. Mittleman, "Using terahertz pulses to study light scattering," *Phys. B* **338**, 92 (2003)
9. A. G. Stepanov, J. Hebling and J. Kuhl, "Efficient generation of subpicosecond terahertz radiation by phase-matched optical rectification using ultrashort laser pulses with tilted pulse fronts," *App. Phys. Lett.* **83**, 3000 (2003)
10. J. Hebling, A. G. Stepanov, G. Almasi, B. Bartal and J. Kuhl, "Tunable THz pulse generation by optical rectification of ultrashort laser pulses with tilted pulse fronts," *App. Phys. B* **78**, 593 (2004)
11. K.-L. Yeh, M. C. Hoffmann, J. Hebling and K. A. Nelson, "Generation of 10 μ J ultrashort terahertz pulses by optical rectification," *App. Phys. Lett.* **90**, 171121 (2007)
12. D. A. Bryan, R. Gerson, H. E. Tomaschke, "Increased optical damage resistance in lithium niobate," *Appl. Phys. Lett.* **44**, 847 (1984)
13. G. Gallot and D. Grischkowsky, "Electro-optic detection of terahertz radiation," *J. Opt. Soc. Am. B* **16**, 1204 (1999)

Radar Cross Section Measurements Using Terahertz Waves

14. D. Turchinovich and J. I. Dijkhuis, "Performance of combined [100]–[110] ZnTe crystals in an amplified THz time-domain spectrometer," *Optics Communications* **270**, 96 (2007)
15. G. Zhao, M. Mors, T. Wenckebach and P. C. M. Planken, "Terahertz dielectric properties of polystyrene foam," *J. Opt. Soc. Am. B* **19**, 1476 (2002)
16. E. F. Knott, "Radar cross section measurements," Van Nostrand Reinhold, New York, 1993
17. D. L. Mensa, "High resolution radar cross-section imaging," Artech House, Boston, 1991
18. N. J. Willis, "Bistatic Radar", 2nd Edition, Technology Service Corporation, 1995.
19. J. A. Stratton, "Electromagnetic Theory," McGraw-Hill, New York and London, 1941

1. Introduction

Radar cross sections (RCS) are important for detecting aircrafts, ships and other targets as well as for counter measures such as RCS reduction and stealth. Terahertz (THz) waves provide a convenient, fast and precise method to measure multiband RCS of scale models in tabletop experiments [1,2]. Terahertz waves also allow for a more detailed target description by bidirectional reflection, absorption and transmission measurements. Also broadband frequencies allow for spectral analyses of e.g. explosives. The penetration of THz waves through cloth and other materials also allow for detection of hidden objects.

In this work we measure THz RCS of scale models and present polar and azimuthal angle and time resolved RCS plots of F-16 and F-35 fighter aircraft models rotated on a pedestal. The time domain sub-ps resolution allows for sub-mm range resolution that can be found in modern software defined radars. The range, polar and azimuthal RCS plots are analogous to inverted synthetic aperture radar images (ISAR) in three dimensions [3,4,5]. The resulting RCS and ISAR images can be compared to measurements on real aircrafts, ships and other platforms by simple scaling. Scattering of THz waves by conducting and dielectric objects is also an area of intensive investigation both on grounds of theory [6] and experiment [7,8].

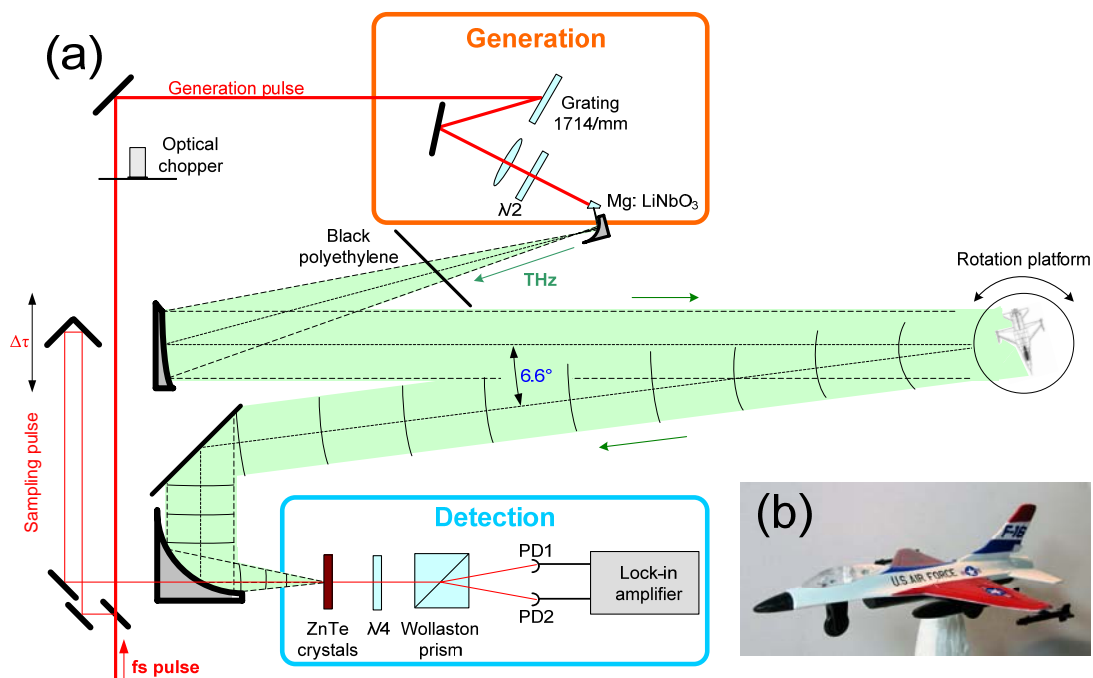


Fig. 1. (a) Schematic diagram of the THz radar cross section setup. (b) 10.2 cm-long 1:150-scale metal model of aircraft fighter F-16.

2. Experimental details

A schematic diagram of our terahertz radar cross section setup is shown in Fig. 1. A regenerative Ti:sapphire femtosecond laser amplifier delivers ~ 35 fs, 2.9 mJ pulses with center wavelength of 800 nm at a 1 kHz repetition rate. The laser output is split into a source beam for THz pulse generation and a gating beam for THz detection by free space electro-optic sampling. Terahertz waves are generated by optical rectification in lithium niobate LiNbO_3 crystal applying the tilted pulse front method [9,10,11]. The intensity front of fs pulses is tilted by a 1714 line/mm grating and imaged by a 75 mm lens, with demagnification of 2, onto the front surface of a stoichiometric LiNbO_3 crystal at room temperature. The LiNbO_3 crystal was doped with 1% of MgO to prevent photorefractive damage [12]. The highest terahertz peak electric field achieved in our setup are round 40 kV/cm, limited predominantly by the high angular and material dispersion inside the LiNbO_3 crystal of the 60 nm-FWHM pump pulses. The near-infrared light transmitted through the LiNbO_3 crystal is blocked by a black polyethylene sheet, transmissive to the THz pulse. A pair of off-axis parabolic mirrors with focal lengths of 25.4 mm and 516.8 mm and diameters of 25.4 mm and 101.6 mm respectively is used to expand the THz beam and subsequently to collimate it. The wide, collimated THz beam propagates 120 cm towards the target which is placed on a computer-controlled motorized rotation platform. The expansion optics increases the terahertz beam size by a factor of 20, which leads to full width at half maximum of the terahertz electric field at the object distance of 73 mm. The electric field of the THz transient is polarized in the vertical plane. The scattered THz radiation is collected by a 170 mm-diameter flat metal mirror at a distance of 120 cm from the target, and focused using a 25.4 mm-diameter, 152.4 mm-focal length off-axis paraboloidal mirror onto a detection crystal. The scattered THz radiation travels 143 cm before it reaches the detection crystal. The angle between the incident and scattered radiation is 6.6° and therefore our radar cross section measurements are bistatic but at the same time reasonably close to a monostatic radar. All THz and infrared beams propagate at a height of 160 mm above optical table which is sufficient high in order to avoid reflections from the table. The setup is aligned using a big 170 mm-diameter metal mirror in a place of scattering object, which reflects all THz radiation in the direction of the receiver.

Radar Cross Section Measurements Using Terahertz Waves

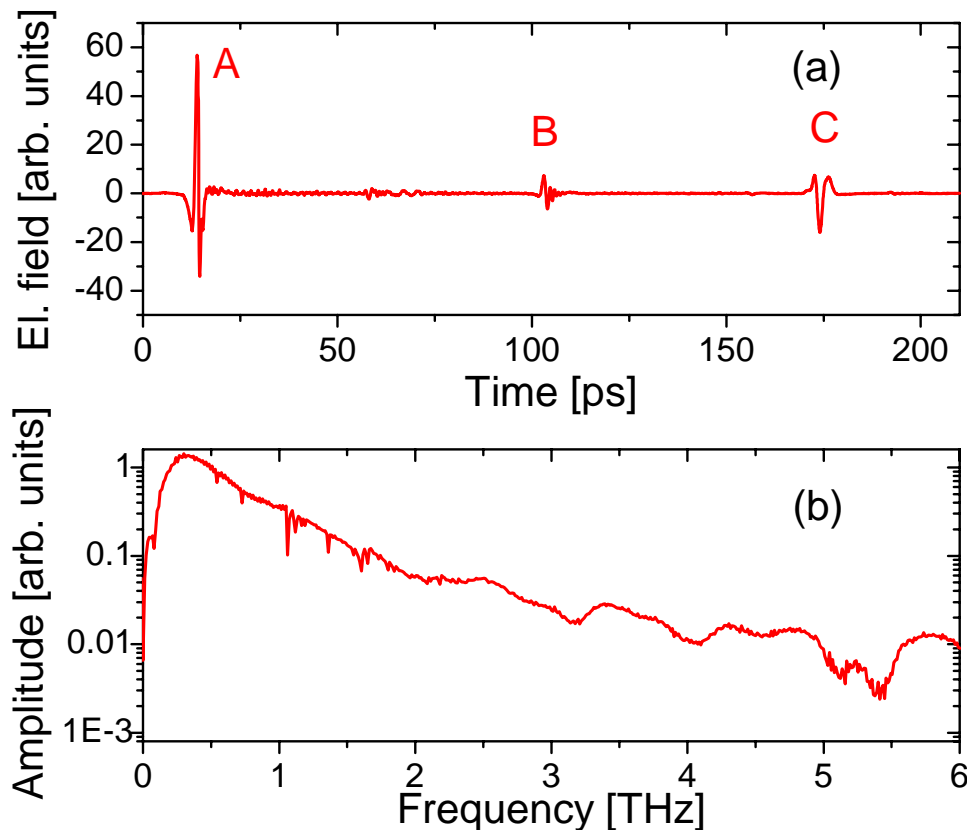


Fig. 2. (a) Terahertz waveform reflected from 170mm-diameter metal flat disk. The transient are (A) the main THz pulse, (B) partial reflection of the main pulse inside the detection crystals, and (C) part of the main pulse undergoing multiple reflections in the LiNbO₃ crystal. (b) Amplitude spectrum of the generated terahertz radiation obtained as a Fourier transform of a 50 ps-broad time window around transient A.

The THz part of the setup was enclosed and purged with dry N₂ to minimize water absorption lines. The 800 nm probe beam was propagated through a small hole in the center of off-axis parabolic mirror for collinear detection. A computer-controlled delay stage was used to map the THz pulse shape. Electric field of the THz transients is detected by free space electro-optic sampling [13] in [110] zinc telluride ZnTe crystal (2 mm-thick). A passive [100] 2mm-thick ZnTe crystal with anti-reflective coating for 800nm light on one side is stacked together with the active crystal to increase temporal separation between the directly transmitted THz pulse (transient A in figure 2(a)) and the pulse that experience two reflections in the detection crystals (transient B in figure 2(a)) [14]. The time delay between these two pulses is 89 ps. The temporal order of incoming pulses is further complicated by an additional THz pulse (transient C in Fig. 2(a)) which experiences multiple reflections inside LiNbO₃ crystal and arrives at detector 160ps after the main pulse. Figure 2(b) shows the amplitude spectrum of the generated THz radiation obtained from a Fourier transform of a 50 ps time window around transient A. The amplitude spectrum extends from 0.02 THz up to 4 THz, but 95% of the generated THz energy lies within 0.1 THz – 1.0 THz range.

The 800-nm beam for THz generation is modulated using an optical chopper at 500 Hz, locked to the laser system trigger so that every second fs pulse is transmitted. The THz waveform is measured using a lock-in amplifier locked to the chopper reference output. The integration time of lock-in was 30 ms. The data acquisition software records data points approximately every 150 ms, which is determined by lock-in amplifier read out time (approx. 50 ms), delay stage step time (approx 50 ms) and lock-in integration time (30 ms).

Target objects are placed on a support column of polystyrene foam, which consists of 97% air or other gases and only 3% polymer, and thus has low refractive index in the THz

range [15]. Furthermore, the polystyrene foam is cut in a shape which resembles a tapered diamond column, which reflects all the THz radiation away from the detector. No signs of volume reflections from thousands of internal cells in the foam structure have been found.

3. Results and discussion

The radar cross section of a scattering target illuminated with radar radiation is a parameter expressed in units of area which describes the intensity of the wave reflected back to the radar. The most general definition of RCS can be written as [16,17],

$$RCS = \lim_{R \rightarrow \infty} 4\pi R^2 \frac{|E_s|^2}{|E_i|^2},$$

where E_i and E_s are the incident and scattered electric fields, and R is the distance between radar and target. In this definition the limiting process is introduced only to ensure that the incident wave is a plane wave, which in the optical design of our setup is fulfilled.

Our setup is designed such that bistatic angle between incident and detected radiation is only 6.6° . The well known Crispin and Siegel monostatic-bistatic equivalence theorem [18] for radar cross section measurement states that for small bistatic angles the bistatic radar cross section of a simple target is equal to monostatic RCS measured on the bisector of the bistatic angle. The theorem is valid for simple objects, for example for a perfectly conducting sphere up to 100° with an error of 3dB, and with more complex shapes up to $\sim 5^\circ$, with constrains being less strict for a large product of object dimensions L and light wave vector k . However the theorem does not hold of objects with multiple reflections (e.g. a corner reflector). The longest THz waves that are generated in our setup have wave vector of $k = 2\pi/\lambda = 2 \text{ mm}^{-1}$ (at $\sim 0.1 \text{ THz}$), so for all the investigated objects ($L > 1 \text{ mm}$) we are in the optical regime ($kL \gg 1$).

We calibrate our measurements with metal spheres of different sizes. In the optical regime the RCS of a perfectly conducting sphere of radius a is πa^2 and is frequency independent.

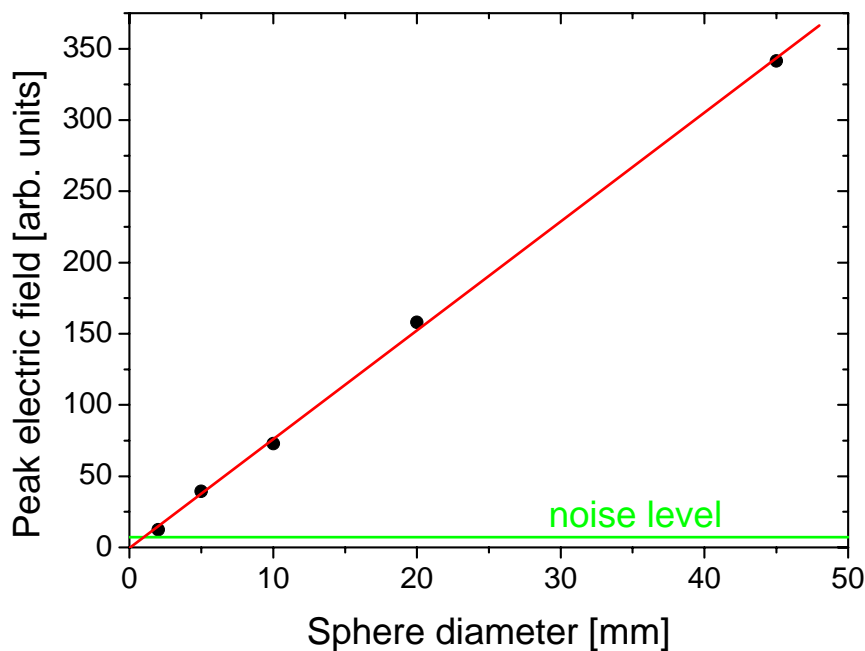


Fig. 3. The peak electric field of THz radiation scattered from a conducting sphere as a function of sphere diameter. The red line shows the best linear fit to the experimental data. The horizontal green

Radar Cross Section Measurements Using Terahertz Waves

line represents the average noise level in single scan measurement. The red and green curves intercept at the point corresponding to a sphere of 0.98 mm diameter.

Figure 3 shows the peak electric field as a function of metal sphere diameter between 2 and 45 mm. The steel spheres are placed on the polystyrene column and centered in the THz beam. The data are results of averaging up to 25 single THz waveforms. Since all the frequency components arrive in phase at the peak of the THz transient, the squared value of the peak electric field E_p accurately represents the energy carried by the pulse and it is less sensitive to noise fluctuations than the integral of the square of pulse waveform. Since $RCS_{\text{sphere}} = \pi a^2$ and $RCS_{\text{sphere}} \sim E_p^2$, we find that $E_p \sim a$. This linear relationship is shown in Fig. 3 from which the coefficient of proportionality is obtained by linear regression (red line). The horizontal green line in figure 3 represents the noise level of a single scan. The smallest detectable sphere in a single scan has a diameter of 0.98 mm.

The metal spheres are simple single-point type scatterers, where the definition of the peak of the electric field is unambiguous. For more complicated structures, which we will be dealing below, the electric field from multiple point scatterers overlap and another method is required for calculating RCS. The frequency-averaged radar cross section is given by:

$$RCS = \pi a^2 \cdot \frac{\int_0^T |E_{\text{object}}(t)|^2 dt}{\int_0^T |E_{\text{cal}}(t)|^2 dt - \int_0^T |E_{\text{bg}}(t)|^2 dt},$$

where $E_{\text{object}}(t)$ is the detected electric from the scattering object, $E_{\text{cal}}(t)$ the electric field scattered by the calibrated spheres of radar cross section of πa^2 , and the $E_{\text{bg}}(t)$ represents background noise. Since we measure not only the intensity of electromagnetic radiation but the field itself we can introduce the frequency resolved RCS defined as follows:

$$RCS(\omega) = \pi a^2 \cdot \frac{|E_{\text{object}}(\omega)|^2}{|E_{\text{cal}}(\omega)|^2 - |E_{\text{bg}}(\omega)|^2},$$

where $E_i(\omega)$ is the Fourier transform of $E_i(t)$.

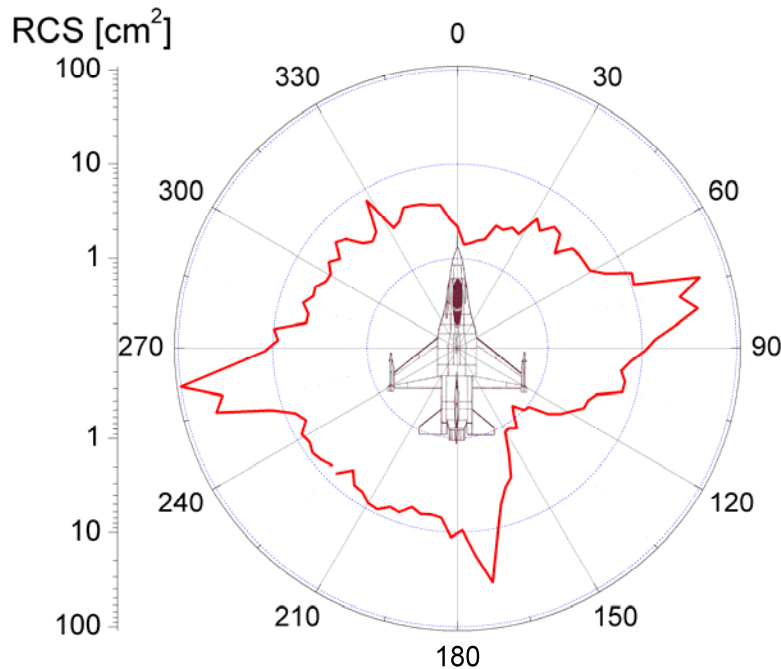


Fig. 4. Frequency-averaged polar RCS of a metal model of aircraft fighter F-16 shown in Fig. 1(b).

Figure 4 shows the measured frequency-averaged polar RCS of a metal model of a aircraft fighter F-16 shown in Figure 1(b). The values of RCS vary from 0.77 cm^2 (seen from a direction between tail and wing) up to 100.9 cm^2 (seen from a wing side). The RCS plot is rotated counter clock wise with respect to the orientation of the symmetry plane. The RCS is asymmetric mainly because the setup is 6.6 bistatic but possibly also due to a minor azimuthal tilt.

Figure 5 shows the logarithm of absolute value of the Hilbert transform of THz waveform vs. polar angle and range (calculated from the time delay and the speed of light), recorded on the F-16 scale model. In such high range resolution maps the single point scatterers are seen as sine functions (sinograms) of rotation angle. However, due to pulse reflections B and C in Figure (2a) some of the sinograms are repeated with corresponding delay. The sinograms can be transformed into two-dimensional images of the target by the inverse radon transform, and our setup thus corresponds to an inverted synthetic aperture radar system (ISAR). ISAR is standard for RCS measurements of ships in the Royal Danish Navy. By scaling we obtain the RCS of real scale models as far as the model is a true copy of the original and assuming that the material properties remain unchanged.

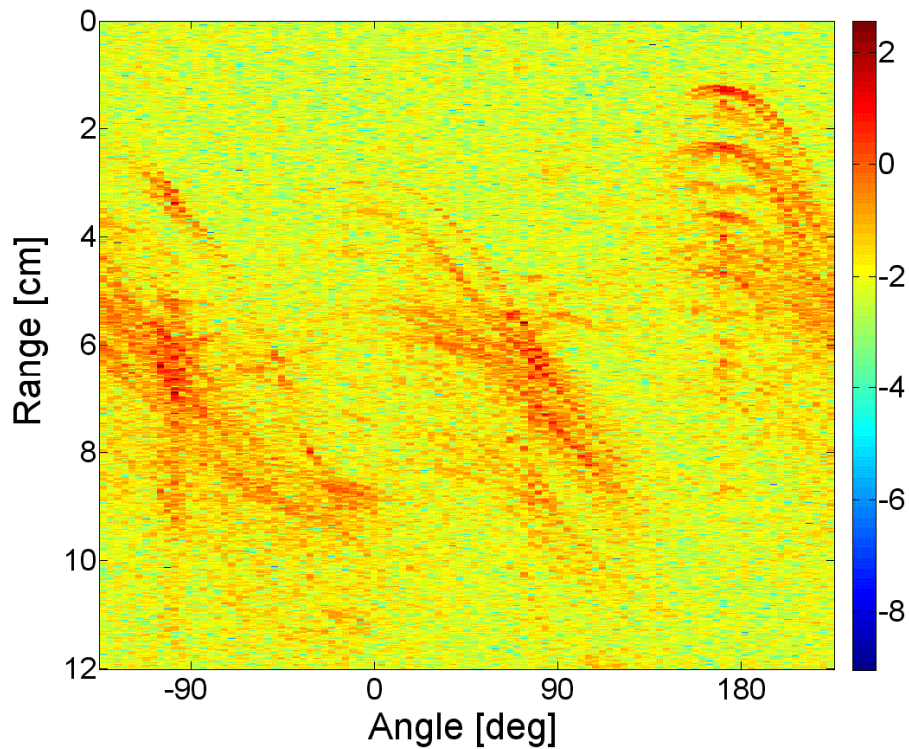


Fig. 5. Logarithm of absolute value of Hilbert transform of THz waveforms scattered from the F-16 scale model for different polar angles.

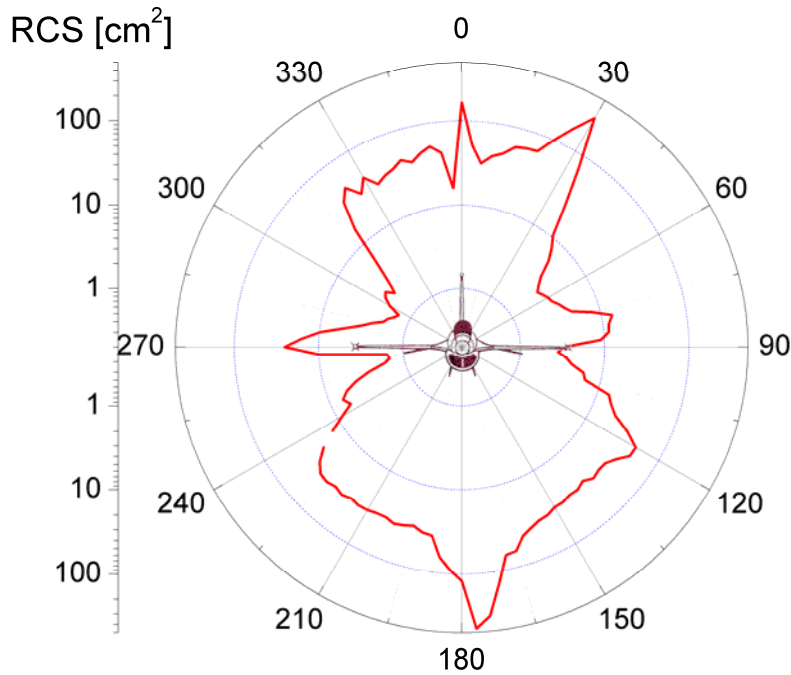
Radar Cross Section Measurements Using Terahertz Waves


Fig. 6. Frequency-averaged azimuthal *RCS* of a metal model of aircraft fighter F16 shown in Fig. 1(b).

Figure 6 shows the measured frequency-averaged *RCS* vs. azimuthal angle of the F-16 model. The *RCS* is generally larger than in the polar plot due to large wing surfaces varying from few cm^2 (seen from a direction seen just below wings) up to 453 cm^2 (seen from below airplane). In Figure 7 the frequency resolved *RCS* is shown for 3 different frequencies: 0.3, 0.6 and 0.9 THz. They vary much more rapidly than the frequency-averaged *RCS* in a non-trivial way because the *RCS* from shapes with different curvatures and corners can be strongly frequency dependent. The results were averaged within a $\pm 20\text{GHz}$ range, in order to minimize the influence of the etalon effect in detection crystal. Figure 8 shows the logarithm of absolute value of Hilbert transform of THz waveform vs. polar angle and time delay. Clear reflections from different parts of airplane, such as wings, tail, main airplane body, are again visible and distinguishable. Elements that reflect in a wide angle range are visible as a long sinograms, while big flat surfaces give high burst of THz signal in a narrow angle interval. Figure 9 shows an example which accurately determines which part of the model is responsible for the high THz reflection. The outer THz trace originates from the reflection off the plastic missile placed at the end of the wing, while the inner trace originates from terahertz scattering off the end of the wing only 3 mm later.

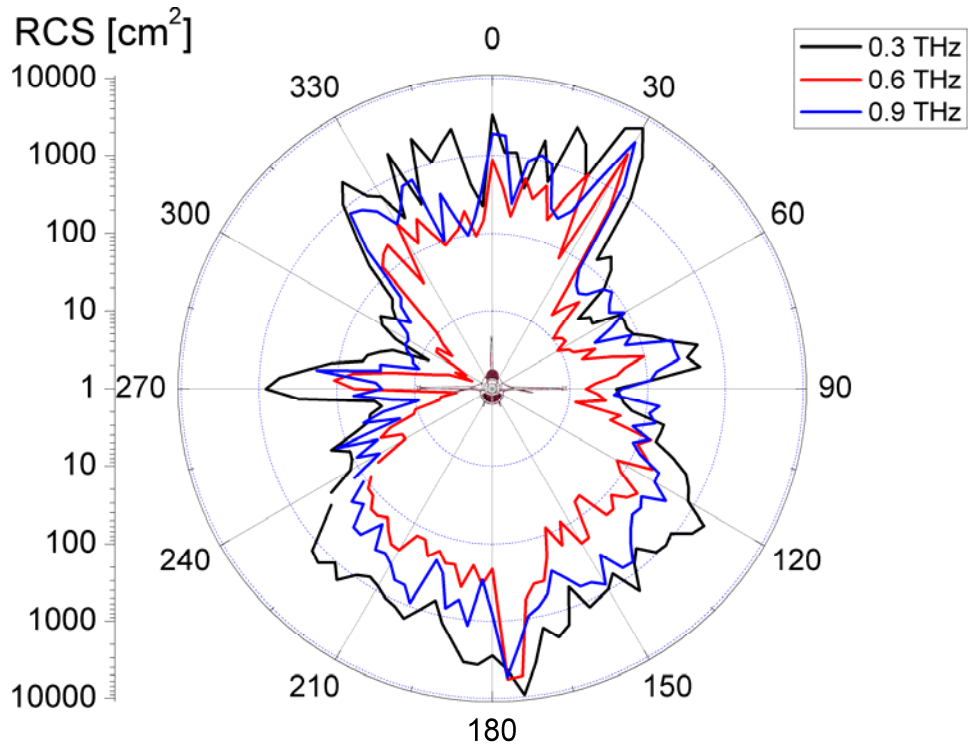


Fig. 7. Frequency-resolved azimuthal RCS of a metal model of aircraft fighter F16 for THz wave frequency of 0.3, 0.6 and 0.9 THz. Presented data are results of averaging within +/- 20GHz range.

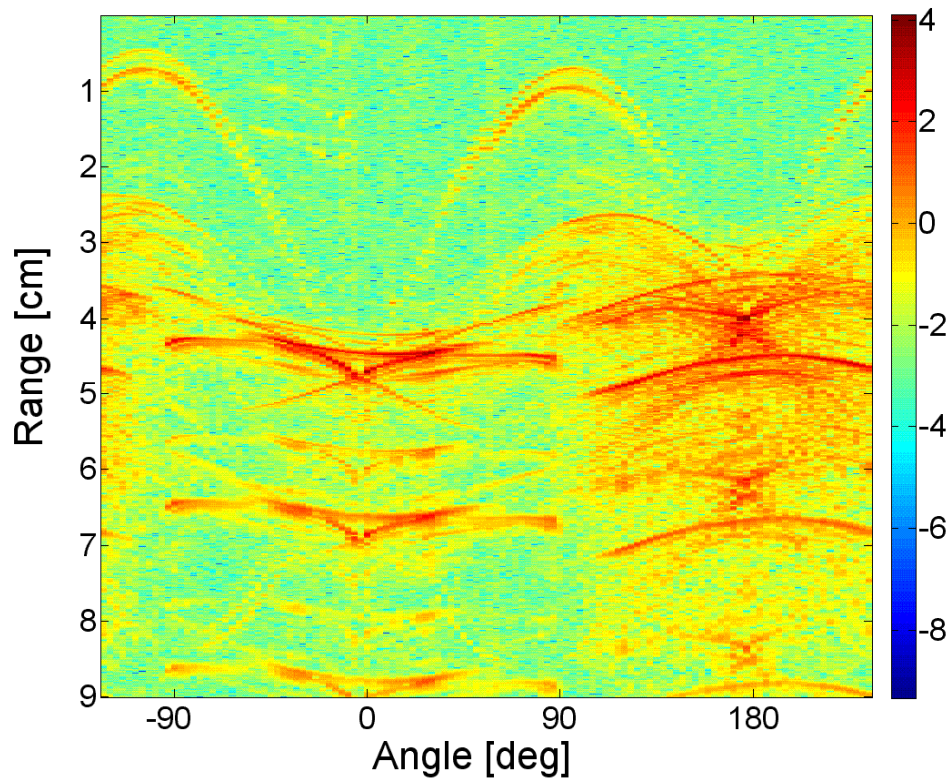


Fig. 8. Logarithm of absolute value of Hilbert transform of THz waveforms scattered from the F-16 scale model for different azimuthal angles.

Radar Cross Section Measurements Using Terahertz Waves

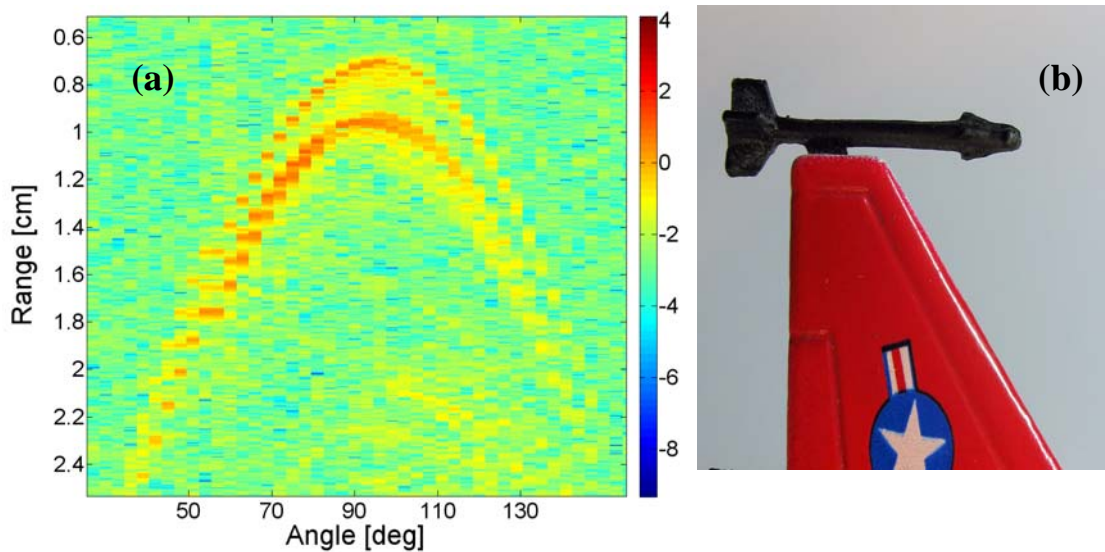


Fig. 9. (a) Magnified part of figure 7 showing two reflections. The first one originates from the plastic missile placed at the end of the wing, and the second one from the wing edge itself, as shown in (b).

Finally, in figure 10 we present frequency-averaged polar RCS of metal 1:150 scale model of aircraft fighter F-35. The airplane is a fifth generation fighter and is designed with application of stealth technology. Even though our model is made out of metal and no radar absorbing materials for RCS minimization are used, the polar RCS measurement for model of F-35 are few times lower than for model of F-16. We have not investigated properties of the paint used for painting models of F-16 and F-35.

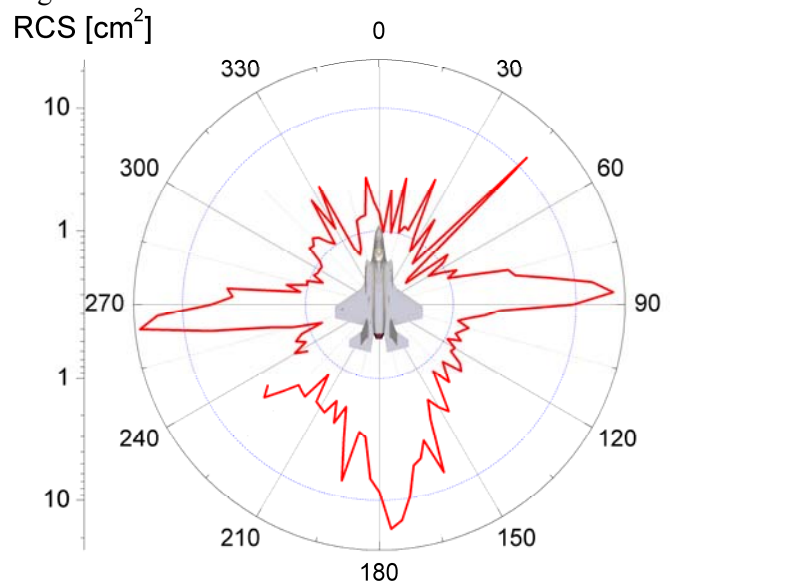


Fig. 10. Frequency-averaged polar *RCS* of a metal model of aircraft fighter F-35

4. Conclusion

We have presented a method for bistatic radar cross section measurements using high-frequency THz waves. The calibrated setup has a transverse resolution of 1 mm and range resolution of 0.1 mm. We have performed a series of RCS measurements of scale

model of aircraft fighters F-16 and F-35 both in the polar and azimuthal orientation. By scaling wavelengths and models to real-scale platforms we can accurately compare to RCS at standard MHz frequencies. Our application of a time domain system allows not only for determination of *RCS* values but also for determination of *RCS* of particular elements of the model from sinograms in high range resolution maps vs. polar and azimuthal angles, and our system thus corresponds to a 3 dimensional ISAR system.

Acknowledgment

We are grateful to the Danish Defense Acquisition and Logistics Organization and Photonics Academy Denmark for financial support.

Radar Cross Section Measurements Using Terahertz Waves

